Memoirs of the School of Engineering, Nagoya University
Vol.44, No.1 (1992) −Research Report−

# The Coherent Structure in a Corner Turbulent Boundary Layer

Ikuo NAKAMURA, Masafumi MIYATA[1], Takehiro KUSHIDA and Takehito YAMAGUCHI[2]

*Department of Mechano-Informatic Systems Engineering*

(Received May 29, 1992)

**Abstract**

The turbulent boundary layer developing along a corner formed by two perpendicular flat plates is examined to clarify the effect of Prandtl's second kind secondary flow on the bursting phenomenon and space correlation contour. Bursting was detected by use of VITA method. Comparison of the two bursting processes of which one is detected far from the corner and the other is detected near the corner has shown definitely the effect of the corner on the bursting process. The space correlation contours have shown the eddy becomes smaller near the corner than that found far from the corner.

## 1. Introduction

As a paradigmatic flow having the secondary flow of Prandtl's second kind, much research has been conducted on the turbulent shear flow along a corner formed by two perpendicular plates[1),2)]. This flow may occur in a boundary layer flow or in a fully developed flow through a square or a rectangular duct. The latter has been extensively examined by use of CFD techniques but so far no satisfactory method is available[3),4)]. In the fully developed turbulent duct flow, having no main free stream in due course, there is no interaction between the boundary layer and the main flow; no displacement and no entrainment of the non-turbulent main flow, and hence no intermittency and no scaling of the outer layer are involved. On the other hand, in the turbulent boundary layer developing along a corner a persistent feature is the interaction between non-turbulent and turbulent fluids. In the previous report we showed that the secondary flow in this case occurs only in the turbulent period[5)]. A pair of weak longitudinal vortices appear only within the turbulent region and this is the main

[1]Department of Mechanical System Engineering, Yamanashi University.
[2]Matsushita Electric Industrial Co. Ltd.

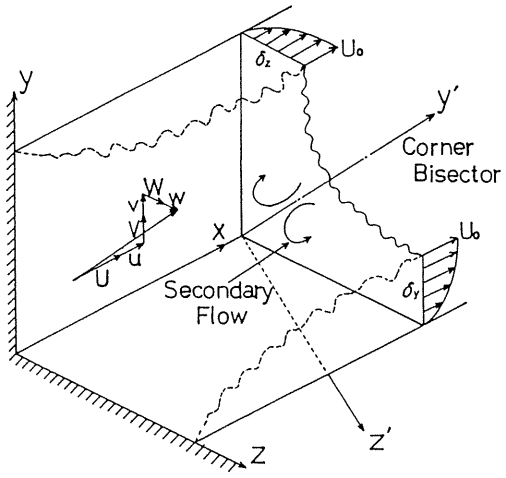


Fig. 1 Flow field and coordinate system.

difference between the secondary flows in a duct and in a corner turbulent boundary layer.

Although a theoretical explanation has not yet been developed on the coherent structure in a flat plate turbulent boundary layer, many experimental and some CFD results have convincingly documented such a structure[6),7)]. Bursting is detected even in a rough wall turbulent boundary layer[8)]. It is therefore interesting to investigate how and to what extent the coherent structure will be modified by the secondary current. In what follows we will describe experimental results of the coherent structure in a corner turbulent boundary layer, shown schematically in Fig. 1.

## 2 Measuring Method

Fig. 1 also contains the coordinate system used, where $y'$ denotes the corner bisector and $z'$ is perpendicular to both $x$ and $y'$ axes. $U_o$ is a constant free stream velocity which was so adjusted to give a unit Reynolds number of $U_o/\nu = 3.5 \times 10^5 \mathrm{m}^{-1}$, where $\nu$ is the kinematic viscosity of air. The working section of an Eiffel type wind tunnel is $0.5 \times 0.3$ m$^2$ and 2 m long. Measurements were performed at a section 1.9 m downstream from the leading edge, using a conventional hot-wire anemometer set.

In order to distinguish a turbulent period from a non-turbulent one, an intermittency function $I$ was generated from a signal proportional to $|du/dt| \propto |\omega|$. The threshold $T_h$ for a turbulence criterion was varied to take into account the effect of turbulence intensity $u'/U_o$, according to the following empirical relation

$$T_h/u' = \{\alpha + \beta(\gamma - u'/U_o)\}, \tag{1}$$

where $\alpha$, $\beta$ and $\gamma$ are constants determined so that the distribution of $\bar{I}$, a time average of $I$, in

the two-dimensional region ($z = 100$ mm) agrees with the results of Kovasznay et al.[9]. We found then that the profiles of average velocities in a turbulent region $U_T$ and in a non-turbulent region $U_P$ agree also with their results. Hereafter suffixes $T$ and $P$ denote averaging in a turbulent and non-turbulent region respectively.

## 3 Velocity Contours

At first, various contours in the $y - z$ plane will be shown to clarify the macroscopic velocity field. Figs. 2a and 2b exhibit the contours of a conventional and a turbulent regional average velocity, $U$ and $U_T$ respectively. In Fig. 2a the contour lines show a characteristic pattern convex to the corner along the bisector, which suggests a pair of counter-rotating longitudinal vortices there. The convex pattern in Fig. 2b is more intensified than that in Fig. 2a, indicating that the vector field ($V_T$, $W_T$) is more definitely associated with the corner vortex. From the definition of $I$, it follows

$$(V, W) = (1 - \bar{I})(V_P, W_P) + \bar{I}(V_T, W_T), \tag{2}$$

hence ($V$, $W$) shows a weaker vortex than ($V_T$, $W_T$) since ($V_P$, $W_P$) does not contain any vortex[5]. A stronger convex pattern observed in Fig. 2b can thus be explained if we assume that distortion of the contour of $U$ or $U_T$ is mainly caused by the longitudinal vortex.

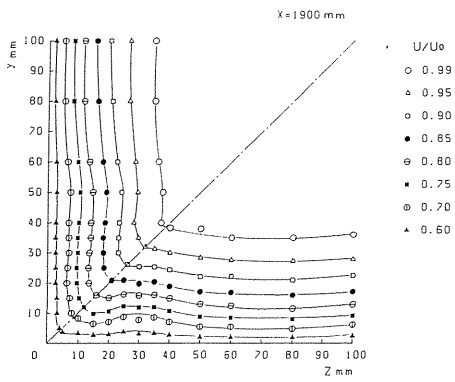


Fig. 2a Contours of conventional mean velocity $U/U_o$.

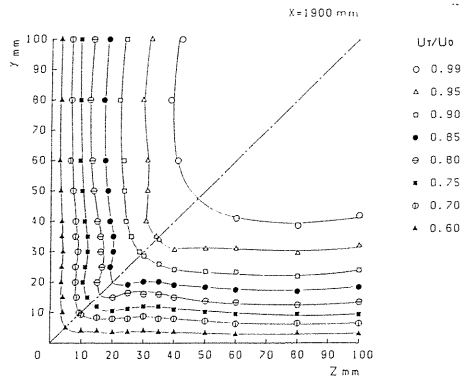


Fig. 2b Contours of turbulent regional average velocity $U_T/U_o$ (Measured only for half the corner region in every contour).

Fig. 2c shows contour lines of a conventional fluctuation $u'/U_o$, where the prime denotes rms value. The convex pattern to the corner vertex is more emphasized in Fig. 2c than those in Figs. 2a and 2b. The contour lines of $u'/U_o$ are, of course, determined by the balance between the convection, diffusion, production and dissipation of the fluctuating energy, but the largest contribution may arise from the convection by ($V$, $W$) field. The mean flow field is

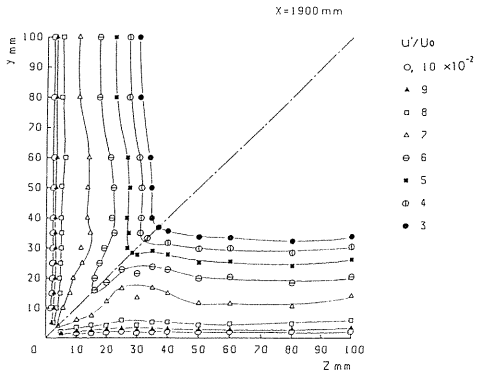


Fig. 2c Contours of conventional fluctuation intensity $u'/U_o$.

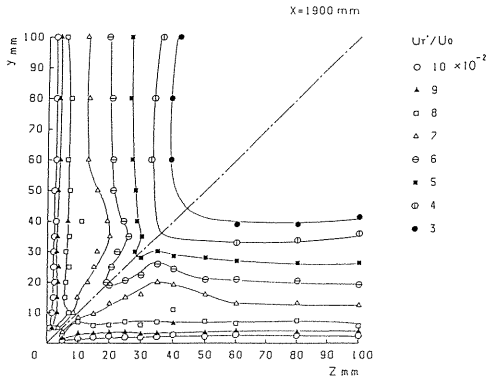


Fig. 2d Contours of turbulent regional fluctuation intensity $u_T'/U_o$.

determined mainly by the larger eddies, but the fluctuating part is dominated by relatively small, energy containing eddies. The larger eddies have larger momentum and the weak secondary flow of the second kind has only a small effect on them. On the other hand, the energy containing eddies interact more strongly with the secondary current, and so the contour lines of $u'/U_o$ show a large deformation. Fig. 2d shows contour lines of $u_T'/U_o$. The convex pattern is most salient in this figure since the secondary flow exists only in the turbulent period and the eddy determining the contour pattern of $u_T'/U_o$ is smaller than the eddy crucial to $U_T/U_o$.

## 4 The Effect of a Corner on Bursting

To detect the bursting event the following short time variance is defined according to Blackwelder and Kaplan[10].

$$\mathrm{var}(x_i,t,T)=\frac{1}{T}\int_{t-\frac{T}{2}}^{t+\frac{T}{2}}u^2(x_i,t')dt'-\left\{\frac{1}{T}\int_{t-\frac{T}{2}}^{t+\frac{T}{2}}u(x_i,t')dt'\right\}^2 \tag{3}$$

and the following burst detecting function $D$ is constructed;

$$D(x_i,t)=\begin{cases}1, \text{ if } \mathrm{var}(x_i,t,T) > ku'^2\\ 0, \text{ if otherwise.}\end{cases} \tag{4}$$

A threshold coefficient $k$ was put as $k=1.0$ and a smoothing time $T$ was determined by the relation $Tu_\tau^2/\nu=20$, where $u_\tau$ is the friction velocity. Using the function $D$, ensemble averaging was carried out over 109 ~ 227 burstings. A burst detecting probe was placed at

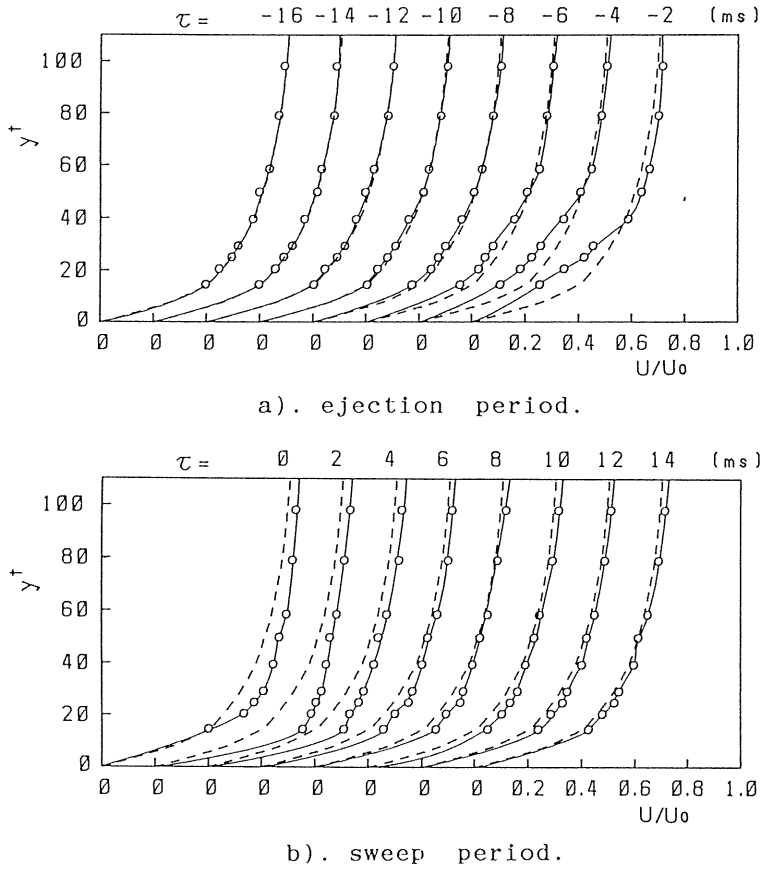


Fig. 3a, b Variations of conditional mean velocity distributions during one bursting cycle at $z = 100$ mm.

$y^+ = 15$ ($y/\delta \simeq 0.025$, $y = 1.0$ mm).

Figs. 3a and 3b show the variations of the conditional mean velocity distributions during one bursting cycle, measured at a time elapsed from the onset of bursting, as well as the conventional mean velocity profiles denoted by dotted line, both obtained in the two-dimensional region. Well known decelerated and accelerated profiles can be seen clearly just before or after $\tau = 0$. Figs. 4a and 4b show similar profiles as Figs. 3a and 3b but were obtained at $z = 25$ mm. A typical ejection process can be seen to occur at nearly $\tau = -4 \sim -2$ msec and then a sweep process follows. The ensemble averaged velocity profiles differ from those in Figs. 3a and 3b. At $\tau = -2$ msec in Fig.4a, a strong shear layer develops near the region $y^+ = 30$ and the velocity above it shows a larger value than the conventionally averaged profile, which leads us to infer that a strong clockwise vortex is generated there. The spanwise vortex parallel to the wall is lifted by the effects of both ejection and secondary current and may cause the high shear layer. Also at $\tau = 2 \sim 4$ msec the profiles exhibit more rapid local acceleration than appears in Fig. 3b.

Figs. 5a and 5b show the bursting process at the position nearer to the corner. Ejection

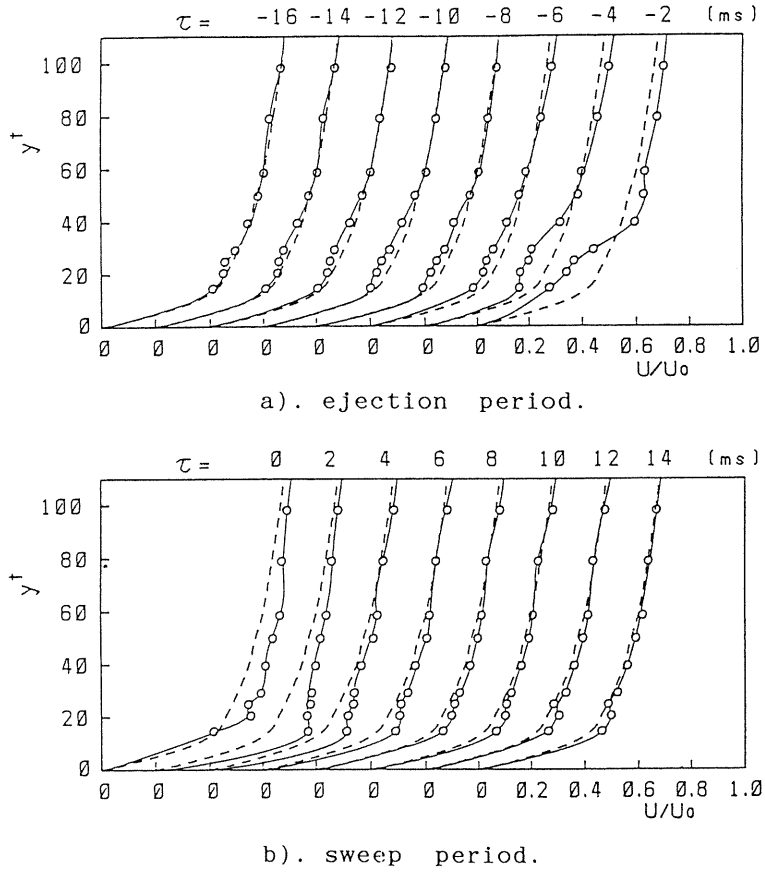


Fig. 4a, b Variations of conditional mean velocity distributions during one bursting cycle at $z = 25$ mm.

and sweep are obvious but the velocity profile shows a more complex pattern. There are two changes, the one occurring in a small scale found at the region near $y^+ = 50$ and the other in a larger scale at near $y^+ = 20 \sim 30$. Specifically, in the sweep stage of $\tau = 0 \sim 4$ msec, there is a definite dent in the ensemble averaged profiles, which implies inflection point instability. This instability will produce strong turbulence in the narrow region both space and time which means the bursting process becomes intermittent near the corner region.

A non-dimensional bursting period $T_b U_o/\delta$ is presented in Fig. 6 as a function of the distance from the corner, where $\delta$ is the boundary layer thickness in the two-dimensional region. Although the value of $T_b U_o/\delta$ scatters considerably the distribution shows some peak at the position where the secondary current leaves the wall.

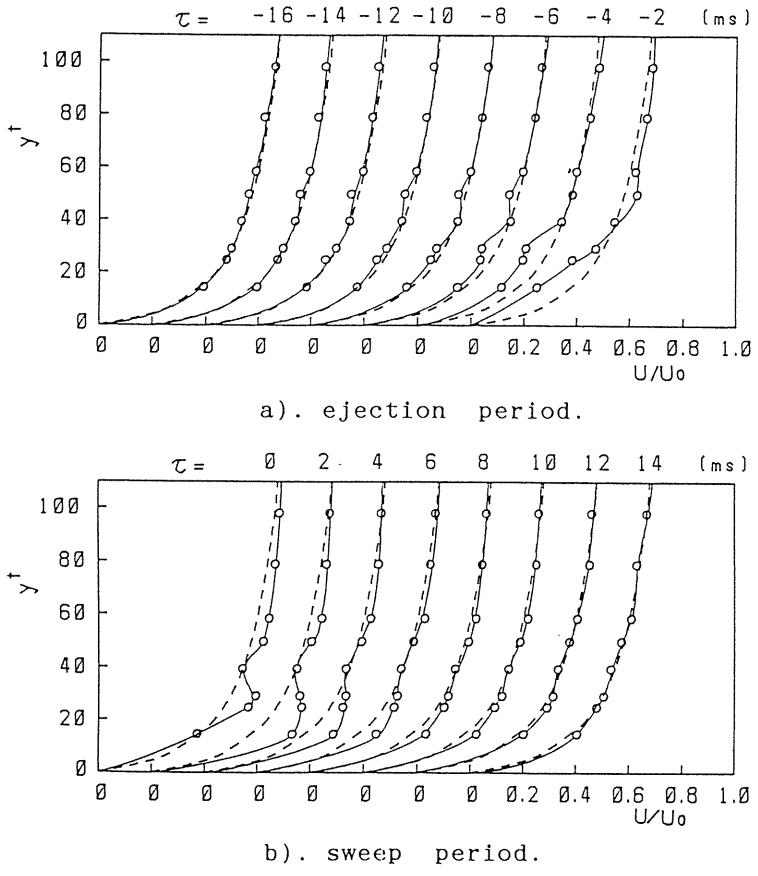


Fig. 5a, b Variations of conditional mean velocity distributions during one bursting cycle at $z = 15$ mm.

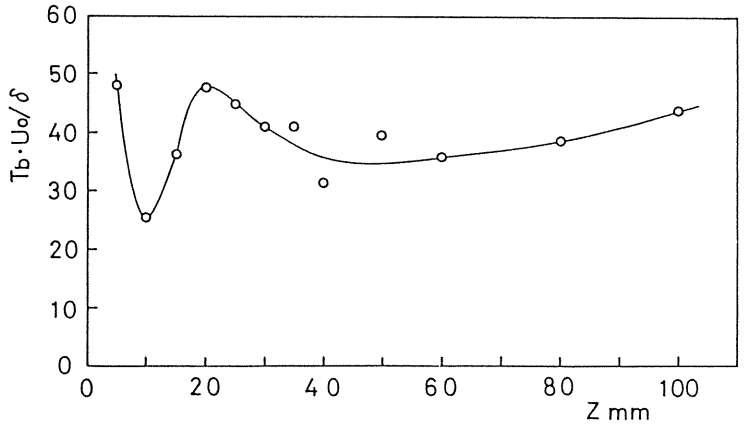


Fig. 6 Distribution of non-dimensional bursting period.

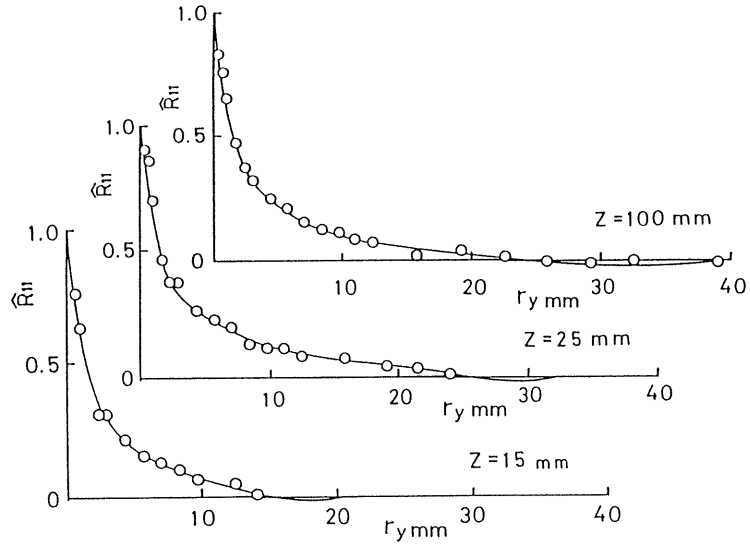


Fig. 7 Distributions of spatial correlation.

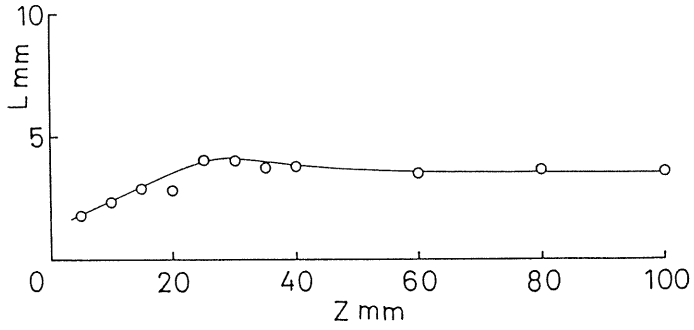


Fig. 8 Distribution of integral length scale.

## 5 The Spatial Correlation and the Eddy Profile

Typical results of the spatial correlation of the $u$-fluctuation are shown in Fig. 7, where probe A was fixed at $y^+ = 15$ and probe B was traversed in the $y$-direction at the same $x$ as probe A. It can be seen in the figure that the length scale becomes smaller as the corner is approached; the distribution of the integral scale presented in Fig. 8 does show that it decreases toward the corner. It means the eddy is suppressed by the space formed by two flat plates which becomes naturally decreases toward the corner.

A clear picture of the eddy shape can be obtained from the iso-correlation contours shown in Figs. 9a, 9b and 9c. $\hat{R}_{11}$ is defined as follows

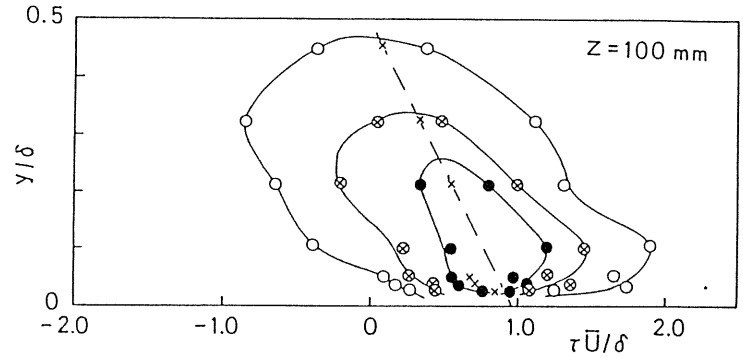


a). z=100 mm.

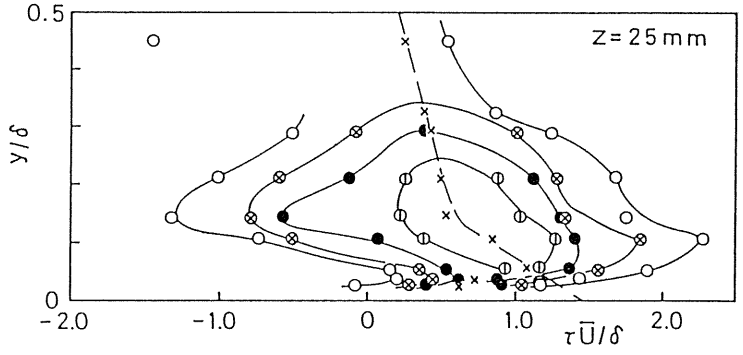


b). z=25 mm.

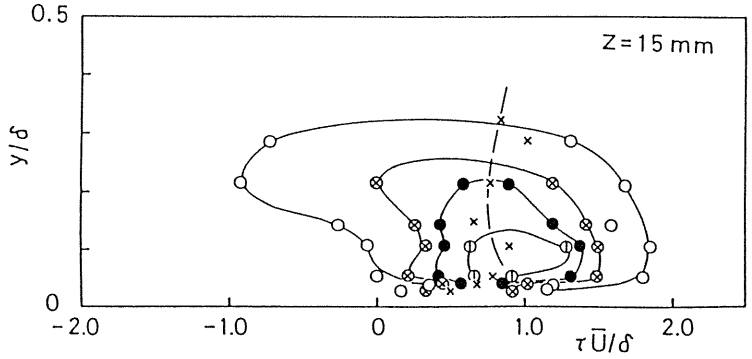


c). z=15 mm.

Fig. 9a, b, c Eddy shapes expressed as conventional iso-correlation curves.

$$\hat{R}_{11} = \overline{u_A(t)u_B(t+\tau)}/u_A' u_B' \tag{5}$$

$$u_A(t) = u(x_A, y_A, z_A, t),\ u_B(t+\tau) = u(x_B, y_B, z_B, t+\tau),$$

where $x_A = 1.9$ m, $x_B = x_A + \delta, y_A = 1.0$ mm ($y^+ = 15$) and $y_B$ is varied while keeping $z_A = z_B$. $U$ is the mean velocity at a position of probe B and $\delta$ is the two-dimensional boundary layer thickness as before. A broken line in each diagram was drawn to pass through a peak point at each height. According to the usual interpretation with the aid of the Lagrangian point of view, iso-correlation contours in Fig. 9a of the two-dimensional region are the results of an eddy having a shape inclined downstream passing the A and B probes. Near the wall, since the angle between the wall and the line connecting the A and B probes is smaller than that of the inclination of the eddy, large correlation occurs at a positive $\tau$ and the situation is reversed when probe B is set far from the wall, leading to large correlation at a negative $\tau$.

Iso-correlation curves at $z = 25$ mm exhibit a distorted shape, especially in the region $y/\delta = 0.15$, as shown in Fig. 9a. Evidently this particular pattern is produced by the secondary current at the corner. Nearer to the corner, i.e. at $z = 15$ mm, the correlation contours show a pattern presented in Fig. 9c and the eddy becomes somewhat smaller due to the constraint of the corner geometry.

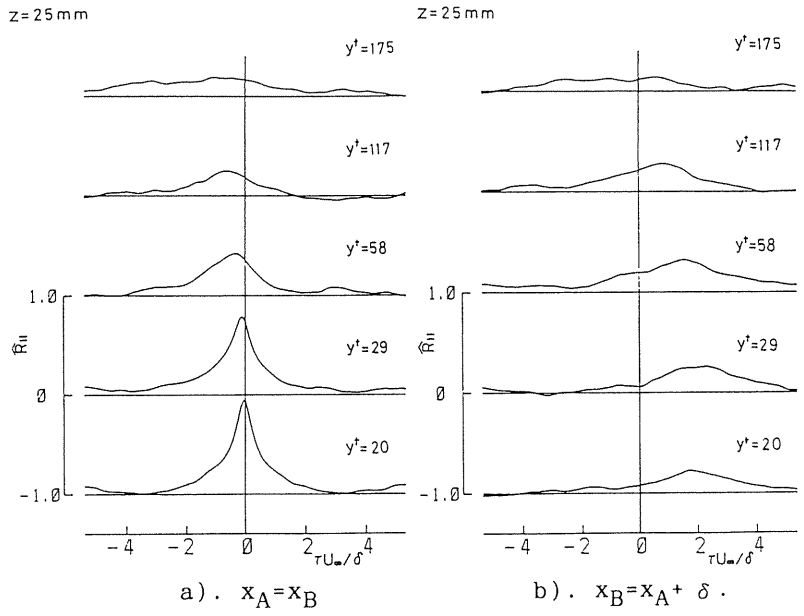


Fig. 10a, b Distributions of space time correlation conditioned by bursting.

In order to examine more details of the relation between bursting and the secondary current, space time correlations conditioned by bursting were measured. An averaging time $T$,

i.e. the bursting period, was estimated by $Tu_\tau^2/\nu = 140$. Typical results of the conditioned space time correlation at $z = 25$ mm are shown in Figs. 10a ($x_A = x_B$) and 10b ($x_B = x_A + \delta$), where the burst detecting probe A is fixed at $y^+ = 15$ in both figures and the values of $y^+$ indicate the heights of probe B. In Fig. 10a, the pattern of the bursting process changes significantly with the height of probe B, but it is not found in Fig. 10b. Also in Fig. 10a the peak value of the conditioned correlation shows a rapid decrease near $y^+ = 58$, indicating a localized character of bursting.

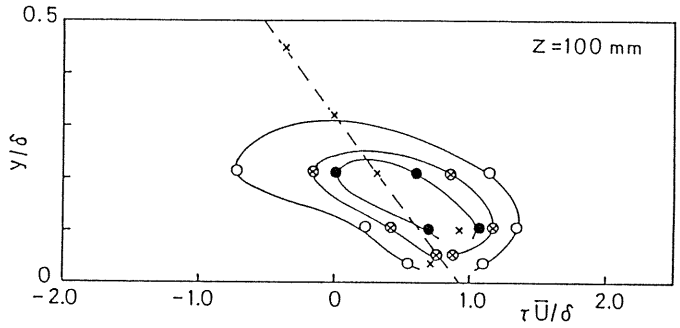


a). z=100 mm.

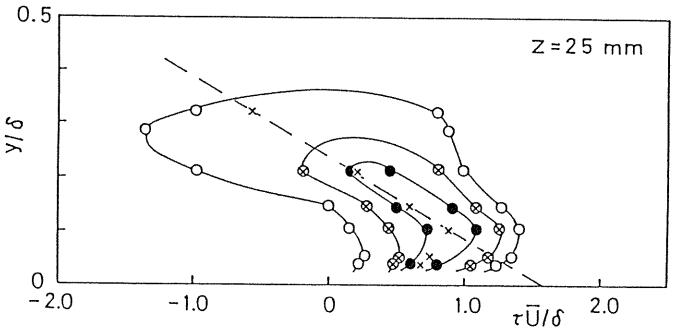


b). z=25 mm.

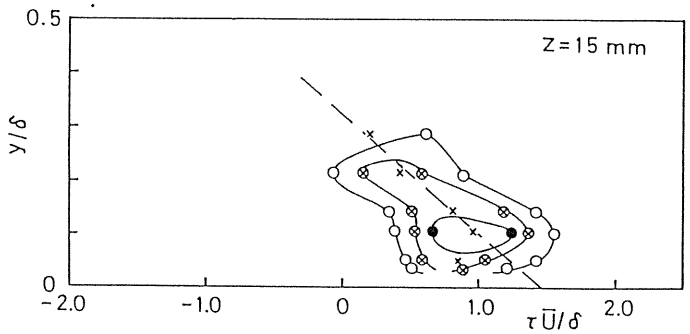


c). z=15 mm.

Fig. 11a, b, c Eddy shapes expressed as iso-correlation curves conditioned by bursting.

From the results mentioned above, iso-correlation contours conditioned by bursting are produced in Figs. 11a, b and c. The dotted line has the same meaning as in Fig. 9. Comparing with the corresponding results in the two-dimensional region (Fig. 11a and Fig. 9a), it is suggested that the eddy conditioned bursting has a smaller scale than that of the conventionally correlated eddy. A similar feature can be found in Figs. 11b and 11c and particularly Fig. 11c ($z=25$ mm) shows a significantly small spatial extent of the coherent eddy, compared it with Fig. 9c.

## 6 Concluding Remarks

Experiment is performed on the corner turbulent boundary layer which has weak vortex of Prandtl's second kind produced by the non-uniformity of turbulence field in the spanwise direction. Detailed measurements using hot wire were performed to obtain the VITA average of streamwise velocity and the space correlation in the various region.

From the experimental results described above, we can say that there is clear evidence of bursting in a turbulent boundary layer along a corner and that the bursting process is evidently modified by the interaction with the secondary current near the corner. The effects of the secondary current appear also in the space time correlation curves and the correlation contours conditioned by bursting show a significantly smaller eddy scale than that of a conventional one.

## References

1) Nikuradse J., *Ing. Arch.*, Vol.1, (1930), p.306.
2) Gessner, F. B., *J. Fluid Mech.*, Vol.58, (1973), p.1.
3) Demuren, A. O. and Rodi, W., *J. Fluid Mech.*, Vol.140, (1984), p.189.
4) Nisizima, S., *Theoretical Computational Fluid Dynamics*, Vol.2, No.1 (1990), p.61.
5) Nakamura, I., Miyata, M., Kushida, T. and Kagiya, Y., *Three-Dimensional Turbulent Boundary Layers*, Springer (1982), p.199.
6) Cantwell, B. J., *Ann. Rev. Fluid Mech.*, Vol.13, (1981), p.457.
7) Moin, P. and Moser, R. D., *J. Fluid Mech.*, Vol.200, (1989), p.471.
8) Osaka, H. and Mochizuki, S., *Trans. JSME*, Vol.52, No.481 (1986), p.3244 (in Japanese).
9) Kovasznay, L.S.G., Kibens, V. and Blackwelder, R.F., *J. Fluid Mech.*, Vol.41, Pt.2 (1970), p.283.
10) Blackwelder, R. F. and Kaplan, R. E., *J. Fluid Mech.*, Vol.76, Pt.1 (1976), p.89.